Conjugation of Kahalalide F with Gold Nanoparticles to Enhance in Vitro Antitumoral Activity

Leticia Hosta,[†,‡] Mateu Pla-Roca,[‡,§] Jordi Arbiol,[||] Carmen López-Iglesias,[⊥] Josep Samitier,[‡,§] Luis J. Cruz,[†] Marcelo J. Kogan,[*,#,▽] and Fernando Albericio[*,†,‡,○]

Institute for Research in Biomedicine; CIBER-BBN, Networking Centre on Bioengineering, Biomaterials and Nanomedicine; Institute for Bioengineering of Catalonia; and Scientific and Technical Services, Barcelona Science Park, University of Barcelona, Baldiri Reixac 10, 08028-Barcelona, Spain, Scientific and Technical Services, University of Barcelona, Lluis Solé i Sabaris 3-5, 08028 Barcelona, Spain, Department of Pharmacological and Toxicological Chemistry, Faculty of Chemistry and Pharmacy, Casilla 233, University of Chile, Olivos 1007, Independencia, Santiago, Chile, Centre for Advanced Interdisciplinary Research in Material Sciences, Av. Blanco Encalada 2008 Santiago, Chile, and Department of Organic Chemistry, University of Barcelona, Martí i Franqués 1, 08028 Barcelona, Spain. Received August 24, 2008; Revised Manuscript Received November 8, 2008

Two Cys-containing analogues of the anticancer drug Kahalalide F are synthesized and conjugated to 20 and 40 nm gold nanoparticles (GNPs). The resulting complexes are characterized by different analytical techniques to confirm the attachment of peptide to the GNPs. The self-assembly capacity of a peptide dramatically influences the final ratio number of molecules per nanoparticle, saturating the nanoparticle surface and prompting multilayered capping on the surface. In such way, the nanoparticle could act as a concentrator for the delivery of drugs, thereby increasing bioactivity. The GNP sizes and the conjugation have influence on the biological activities. Kahalalide F analogues conjugated with GNPs are located subcellularly at lysosome-like bodies, which may be related to the action mechanism of Kahalalide F. The results suggest that the selective delivery and activity of Kahalalide F analogues can be improved by conjugating the peptides to GNPs.

Downloaded via UNIV DE CHILE on September 10, 2019 at 18:54:57 (UTC).
See https://pubs.acs.org/sharingguidelines for options on how to legitimately share published articles.

INTRODUCTION

Nanotechnology offers tremendous potential for medical diagnosis and therapy. Various types of nanoparticles have been explored for biomedical applications (*1*−*3*), having been widely employed in biological systems (*4*−*6*). Nanoparticles have been suggested for imaging (*7*−*13*), screening (*14*), and biosensing (*15*−*17*), not using only gold nanoparticle optical properties but also electrical (*18*−*23*), and furthermore are known to carry higher payloads of drugs than other vehicles and are currently used in gene and drug delivery (*24*−*26*), as well as in cancer diagnostics and therapeutic applications (*27*−*29*). Gold NPs (GNPs) display several features that make them well-suited for biomedical applications, including straightforward synthesis, stability (*30*), and the facile ability to incorporate secondary tags such as peptides targeted to specific cell types to afford selectivity (*31, 32*). On the other hand, GNPs have been used in photothermal therapy for the destruction of cancer cells or tumors. When irradiated with a focused laser in the near-infrared region (NIR) of suitable wavelength, targeted aggregates of GNPs, nanorods, or nanoshells can kill bacteria (*33*) and cancer cells (*34*).

The conjugation of GNPs to an antitumoral drug could play two parallel roles: to enhance the delivery of a drug to the cell by presenting numerous peptide copies anchored to the nanoparticle surface and to help in the delivery of the nanoparticle to the pathological cell favoring the local aggregation of nanoparticles in tumor cells by increasing absorption in the NIR where tissues present low NIR region radiation absorption, after irradiation.

Nanobiotechnology is expected to widen the therapeutic index of current cancer therapies. For example, tumor-targeting drug delivery vectors are now approaching "true" nanometer size, which allows them to arrive in close proximity to several biological targets (*35*). Cellular delivery involving the transfer of various drugs and bioactive molecules (e.g., peptides, proteins, and DNA) through the cell membrane into the cytoplasm has generated great interest because the general administration of drugs and biomolecules suffers from inefficiency and enzymatic degradation, among other problems. Hence, there is a pressing need to develop safe and efficient transport vehicles to deliver drugs into cells (*36*). Taking into account the advantages of GNPs for drug delivery, in this work we have conjugated a Kahalalide F analogue, an antitumoral drug candidate, with GNPs to enhance the delivery of Kahalalide F to tumoral cells by increasing its cytotoxic effect. Kahalalide F is a marine cyclodepsipeptide isolated from a mollusk, *Elysia rubefescens*, with antitumoral activity (*37*). Two synthetic diasteromeric analogues of the Kahalalide F (Figure 1) were synthesized and conjugated with GNPs. Kahalalide F is the most bioactive member of the Kahalalide family of peptides. The presence of the compound appears to cause alterations in cell lysosomes, meaning that lysosomes become a target for Kahalalide F action (*38, 39*). Kahalalide F exerts a potent in vitro cytotoxic activity toward several tumor cell lines and specimens derived from various human solid tumors. In contrast, nontumor cell lines are 5 to 40 times less sensitive to Kahalalide F (*40*).

* To whom correspondence should be addressed. Phone: +5629782897, email: mkogan@ciq.uchile.cl. Phone: +34934037088, Fax: 0034 934037126, e-mail: albericio@pcb.ub.cat.

[†] Institute for Research in Biomedicine, Barcelona Science Park.

[‡] CIBER-BBN, Networking Centre on Bioengineering, Biomaterials and Nanomedicine, Barcelona Science Park.

[§] Institute for Bioengineering of Catalonia, Barcelona Science Park.

[||] Scientific and Technical Services, University of Barcelona.

[⊥] Scientific and Technical Services, Barcelona Science Park.

[#] University of Chile.

[▽] Centre for Advanced Interdisciplinary Research in Material Sciences.

[○] Department of Organic Chemistry, University of Barcelona.

10.1021/bc800362j CCC: $40.75 © 2009 American Chemical Society
Published on Web 12/12/2008

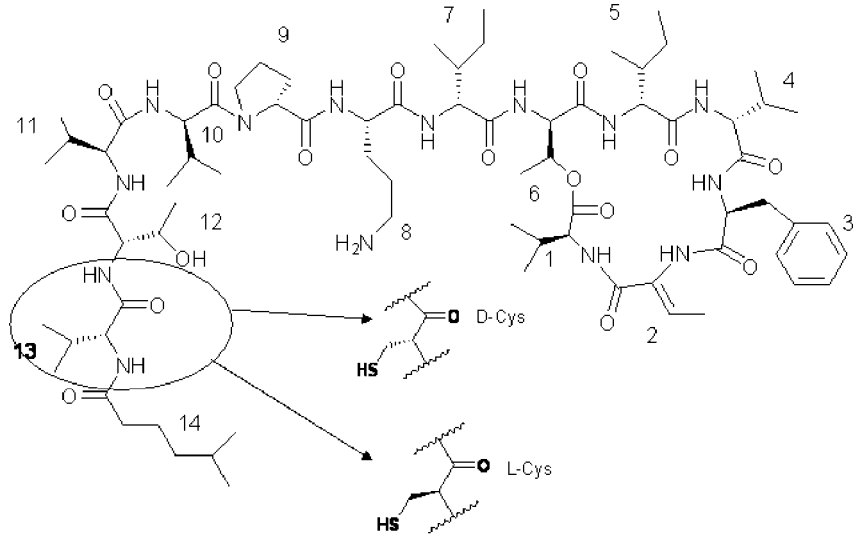

Kahalalide F: 5-MeHex[14]-**DVal[13]**-Thr[12]-Val[11]-DVal[10]-DPro[9]-Orn[8]-DalloIle[7]-DalloThr[6](&)-DalloIle[5]-DVal[4]-Phe[3]-(Z)Dhb[2]-Val[1]&

P1: D-Val[13] is replaced by D-Cys; **P2:** D-Val[13] is replaced by L-Cys

Figure 1. Structures of Kahalalide F, **P1**, and **P2**; amino acid sequences and linear cyclopeptides are represented in a one-line text formula using the protocol of Spengler et al. (*43*).

Kahalalide F shows in vitro activity against prostate and colon cancer cells, and to a lesser extent, antiviral, antifungal, and bactericide activity (*41*). Two clinical phase I trials in adult patients with advanced prostate cancer and pretreated solid tumors have established the recommended dose for two distinct treatment regimes (once a week and five consecutive days every 3 weeks) (*40, 42*). Kahalalide F phase II clinical trials in hepatocellular carcinoma, non-small cell lung cancer (NSCLC), and melanoma finished in 2006. Moreover, Kahalalide F is being tested in phase II clinical trials in patients with severe psoriasis.

Herein, we report on the ability of Kahalalide F analogue−GNP complexes to enter HeLa cells. The penetration, localization, and in vitro cytotoxicity of the conjugates in HeLa cells were evaluated.

MATERIALS AND METHODS

Materials. Cl-TrtCl-resin (100 mg, 1.56 mmol/g), protected Fmoc-L-amino acids and Fmoc-D-amino acids derivatives, were purchased from Iris Biotech GmbH (Marktredwitz, Germany), Luxembourg Industries (Tel-Aviv, Israel), Neosystem (Strasbourg, France), Calbiochem-Novabiochem AG (Laüfelfingen, Switzerland), and Bachem AG (Bubendorf, Switzerland). Diisopropylcarbodiimide (DIC) was obtained from Fluka Chemika (Buchs, Switzerland); HOAt, from GL Biochem (Shanghai, China); PyBOP, from Calbiochem−Novabiochem AG; and *N,N*-diisopropylethylamine (DIEA), from Merck (Darmstadt, Germany). Solvents for peptide synthesis and RP-HPLC were obtained from Scharlau (Barcelona, Spain). Trifluoroacetic (TFA) acid was supplied by KaliChemie (Bad Wimpfen, Germany). Other chemicals used were obtained from Aldrich (Milwaukee, WI) and were of the highest purity commercially available.

Peptide Synthesis and Purification. Both peptides were synthesized on solid phase using a method previously reported by our group (*44*). HPLC was performed using a Waters Alliance 2695 (Waters, MA) chromatography system with a PDA 995 detector, a reverse-phase Symmetry C_{18} (4.6 × 150 mm) 5 μm column, and a linear gradient of MeCN with 0.036% TFA into H_2O with 0.045% TFA. The system was run at a flow rate of 1.0 mL/min. HPLC-MS was performed using a Waters Alliance 2796 with a UV/vis detector 2487, ESI-MS Micromass ZQ (Waters) chromatography system, a reverse-phase Symmetry 300 C_{18} (3.9 × 150 mm) 5 μm column, and H_2O with 0.1% formic acid, and MeCN with 0.07% formic acid, as mobile phases. Mass spectra were recorded on a MALDI Voyager DE RP time-of-flight (TOF) spectrometer (PE Biosystems, Foster City, CA).

Synthesis of GNPs. GNPs were produced by reduction of hydrogen tetrachloroaurate ($HAuCl_4 \times H_20$) obtained from Aldrich (Milwaukee, WI).

20 nm Nanoparticles. $HAuCl_4 \times H_2O$ (8.7 mg) was added to a sodium citrate solution (100 mL, 2.2 mM) at 150 °C reflux. The reducing agent was added rapidly, and the reaction was allowed to continue under uniform and vigorous stirring until a red wine color was observed (*45*).

40 nm Nanoparticles. Same procedure as above except that a lower concentration of reducing agent was used (100 mL of a 1.22 mM solution of sodium citrate).

Conjugation of Peptides with GNPs. An excess of peptide was used for the conjugation (*6*). Peptide solutions (1 mg/mL in MilliQ water) were added dropwise to 10 mL of GNPs solution at room temperature with magnetic stirring, and agitation was then maintained for 15 min. The conjugates were then purified by dialysis over three days in a Spectra/Por MWCO membrane: 6−8000 against 2.2 mM sodium citrate. The solution was refreshed six times to eliminate the excess peptide (**P1** or **P2**).

UV−visible. UV−vis absorption spectra were recorded at room temperature with a 2501PC UV−vis recording spectrophotometer (Shimadzu Corporation, Kyoto, Japan).

High-Resolution Transmission Electron Microscopy (HR-TEM). Drops of GNPs conjugated to both Kahalalide F analogues under uranyl acetate staining were deposited over carbon-coated Formvar films on copper grids. To obtain the transmission electron microscopy (HRTEM) results, a field emission gun microscope JEOL 2010F was used, working at 200 kV and with a point-to-point resolution of 0.19 nm.

Electron Energy Loss Spectroscopy (EELS). Electron energy loss spectra (EELS) were obtained in a Gatan Image

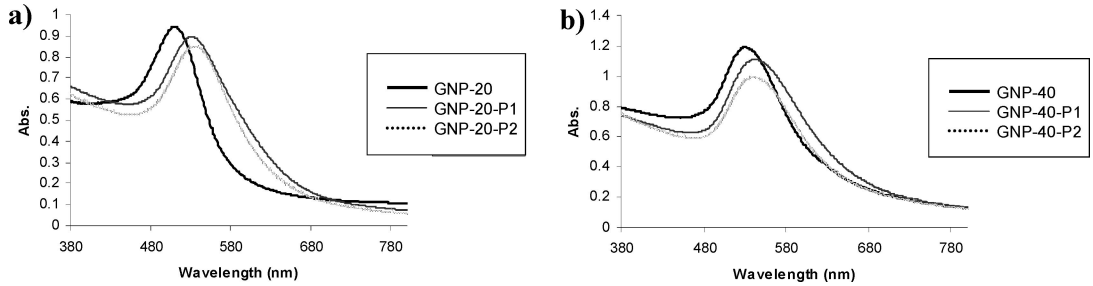

Figure 2. UV−vis spectra of GNPs and their respective conjugates; a shift in the maximum is representative of the conjugation. (a) GNP-20, GNP-20-P1, and GNP-20-P2; and (b) GNP-40, GNP-40-P1, and GNP-40-P2.

Filter (GIF 2000) coupled to the JEOL 2010F microscope, with an energy resolution of 1.2 eV.

X-ray Photoelectron Spectroscopy (XPS). Gold surfaces were purchased from Arrandee (Germany), and PMMA surfaces, from GoodFellow (Huntingdon, United Kingdom). XPS studies were performed by depositing a drop of GNPs or the conjugates over PMMA surfaces, and then drying the samples under reduced pressure before analysis. Gold surfaces functionalized with **P1** were obtained by immersion of **P1** (0.1 mg) in a $CHCl_3$ (1 mL) solution for 24 h.

Cell Culture and Incubation with the Conjugates. HeLa cell line was obtained from ATTC no CCL-2 (Manasas, VA) and maintained in DMEM low-glucose medium (Biological Industries) containing 10% fetal calf serum (FCS), 2 mM glutamine, 50 U/mL penicillin, and 0.05 g/mL streptomycin. For experiments, exponentially growing HeLa cells were detached from the culture flasks using a trypsin−0.25% ethylenediaminetetraacetic acid (EDTA) solution, and the cell suspension was seeded at a concentration of 3.5×10^3 cells/cm^2 onto glass coverslips (Nalge Nunc International, Rochester, NY). Experiments were carried out 24 h later, when the confluence was approximately 70−80%. Non-adherent cells were washed away and attached cells were incubated at 37 °C in 5% CO_2 in DMEM with a known concentration of GNPs.

WST-1 Assay. HeLa viability in the presence of unconjugated or conjugated nanoparticles was tested using a WST-1 assay, including a control with no nanoparticles added. For each assay, 3.5×10^3 cells/cm^2 were seeded onto a 96 well plate (Nalge Nunc) and cultured for 24 h. The conjugates were added in a 1:4 (conjugate/DMEM) ratio. Cells were incubated for 24 h at 37 °C under a 5% CO_2 atmosphere. After 20 h, 10 μL of WST 1 were added. The cells with the conjugate solutions were incubated for another 4 h. Cell viability is expressed as a percentage ratio of cells treated with the different compounds against untreated cells.

Confocal Laser Scanning Microscopy (CLSM). For the cellular localization of GNP conjugates, HeLa cells were plated on glass coverslips, grown to 60% confluence, and then incubated (at 37 °C under a 5% CO_2 atmosphere) with either **P1**− and **P2**−nanoparticle conjugates for 24 h. At indicated time points, the coverslips were rinsed extensively with phosphate-buffered saline (PBS), and the cells were fixed with 4% paraformaldehyde in PBS for 20 min at room temperature and then rehydrated in PBS.

Once the cells were fixed, the coverslips with cells were mounted onto glass slides with Mowiol mounting media (Calbiochem, CA), and then allowed to dry overnight prior to microscopy analysis. The samples were examined using an Olympus Fluoview 500 confocal microscope with a 60×/1.4 NA objective.

Nanoparticle Localization by Transmission Electron Microscopy (TEM). HeLa cells were incubated with conjugated or unconjugated gold nanoparticles for 24 h. Cells were fixed with 2.5% glutaraldehyde in phosphate buffer, and then kept in the fixative at 4 °C for 24 h. The cells were then washed with the same buffer, and postfixed with 1% osmium tetraoxide in the same buffer containing 0.8% potassium ferricyanide at 4 °C. The samples were then dehydrated in acetone, infiltrated with Epon resin for 2 days, embedded in the resin, and polymerized at 60 °C for 48 h. Ultrathin sections were obtained using a Leica Ultracut UCT ultramicrotome, and then mounted on Formvar-coated copper grids. The sections were stained with 2% uranyl acetate in water and lead citrate, and then observed under a JEM-1010 electron microscope (Jeol, Japan).

RESULTS AND DISCUSSION

Modification of Kahalalide F for Conjugation with GNPs. Two Kahalalide F analogues **P1** and **P2** (Figure 1) were synthesized and conjugated to NPs. For conjugation with GNPs, a free thiol containing Cys that facilitates the attachment to the gold surface was introduced in the peptide sequence. In **P1**, the D-^{13}Val was replaced by a D-Cys residue that does not seem to be crucial for biological activity. To determine whether the Cys configuration affects toxicity, **P2** was obtained from where the D-Val had been replaced by a L-Cys instead a D-Cys, as in **P1**.The change of chirality from D-Cys (**P1**) to L-Cys (**P2**) should induce a decrease in antitumoral activity from **P1** to **P2**. These results are in agreement with Jimenez et al., who reported that when the chirality of a residue of the Kahalalide F tail changes, the activity decreases (*46*).

P1 and **P2** were synthesized using a Fmoc/tBu solid-phase synthesis strategy (Supporting Information) (*44*).

Conjugation of P1 and P2 with GNPs. GNP cellular uptake is heavily dependent on nanoparticle size (*47*). In this work, **P1** and **P2** were conjugated to two different GNP sizes, i.e., 20 and 40 nm (GNP-20 and GNP-40, respectively) obtaining conjugates GNP-20-P1, GNP-20-P2, GNP-40-P1, and GNP-40-P2 in order to determine the influence of nanoparticle size on the penetration and cytotoxicity of the conjugates.

GNPs were obtained via the sodium citrate reduction method (*48*−*52*), which allows the synthesis of clusters between 6 and 60 nm by adding varying amounts of the reducing agent. The GNPs were characterized by UV−vis and TEM (Supporting Information). The peptide-capped GNPs were prepared by mixing a colloidal gold solution with an excess of peptide to obtain functionalized gold surfaces. The conjugates were exhaustively characterized by using UV−vis spectroscopy, amino acid analysis (AAA), transmission electron microscopy (TEM), electron energy loss spectroscopy (EELS), and X-ray spectroscopy (XPS).

Characterization of Conjugates. *UV*−*visible Spectroscopy.* UV−vis spectra of GNPs were taken (Figure 2). The characteristic correlation between surface plasmon resonance band and nanoparticle size (*53*) (520 nm for the 20 nm size, and 530 nm for the 40 nm size) was observed. In peptide−GNP conjugates, the wavelength of maximum absorption was shifted to longer

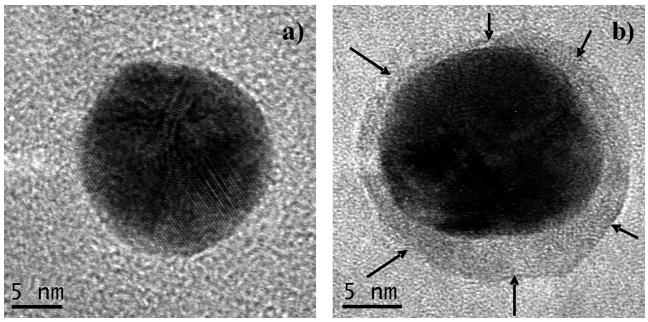

Figure 3. (a) bare GNP-20 and (b) GNP-20-P1.

wavelengths (Figure 2), which could be explained by the capping of the nanoparticle surface with the peptide molecules.

High-Resolution Transmission Electron Microscopy (HR-TEM). Figure 3 shows high-resolution TEM micrographs (HRTEM) of GNP-20 (Figure 3a) and GNP-20-P1 (Figure 3b). The presence of a layer around the nanoparticle core (Figure 3b) corresponding to the peptide was observed following uranyl acetate staining. As observed, the peptide covered the whole surface of the nanoparticle and increased the hydrodynamic size of the peptide-capped nanoparticle by 6 nm (the GNP metallic core as 20 nm in diameter, while the GNP-20-P1 was approximately 25 nm). The capping of GNPs by the adsorption of proteins was observed by TEM by other authors (*54*). However, in our case, although the nanoparticle was capped with a short peptide (approximately 1 nm long in an extended form), the formation of a wide layer (5 nm) was observed. This result led us to conclude that the nanoparticle was capped by a peptide multilayer.

Further characterization of the conjugates was carried out as described next. EELS (electron energy loss spectroscopy) and XPS (X-ray photoelectron spectroscopy) were used to confirm the presence of S−Au bonds on the surface, and amino acid analysis was performed to determine the number of peptide molecules that were conjugated to the GNPs.

Electron Energy Loss Spectroscopy (EELS). An accurate analysis of the electron energy loss near edge spectra (ELNES) at the Au $O_{2,3}$ edge (54 eV), showed that the shape of the edge changed slightly when the spectrum was obtained on the unconjugated GNPs with regard to the **P1**-conjugates (Figure 4b,e, respectively). The change of the ELNES shape at the Au $O_{2,3}$ edge can be directly attributed to a bonding variation on some of the Au surface atoms. To determine the cause of this bonding variation, we also analyzed the S $L_{2,3}$ edge placed at around 165 eV. In this case, energy-filtered spectra obtained on the Au conjugated nanoparticle surfaces showed a clear signal around 165 eV (Figure 4f), indicating the presence of S atoms on the Au nanoparticle surface as detailed by Olmedo et al. (*55*).

The same energy region analyzed on the unconjugated nanoparticle surfaces showed a noise signal only, as indicated in Figure 4c. Given that the unconjugated sample was assumed to have a low quantity of S atoms, it was used to evaluate the signal-to-noise ratio at the S $L_{2,3}$ energy region. The average ratio between the maximum on the Au $O_{2,3}$ peak and the maximum noise signal after background subtraction found at the S $L_{2,3}$ energy region was 4×10^{-3} for the unconjugated nanoparticles. However, values of up to 8×10^{-3} were found for the functionalized nanoparticles, indicating that the increase in the signal-to-noise ratio may be due to bound S atoms. This last result corroborates the presence of S atoms on the Au surface, which would be responsible for the slight change in the Au $O_{2,3}$ ELNES spectra due to their bonding. Consequently, the presence of bound S atoms would indicate the functionalization of the GNPs with P1.

X-ray Photoelectron Spectroscopy (XPS). The gold colloids were further characterized by X-ray photoelectron spectroscopy (XPS). XPS studies were carried out on **P1**-conjugate and unconjugated gold nanoparticles deposited on polymethylmethacrylate surfaces (PMMA). This polymeric surface was used to minimize interference coming from the substrate, a problem commonly observed when sulfur-containing compounds are analyzed on silicon surfaces (*56*).

The S_{2p} spectrum gave a weak signal due to the presence of only one sulfur atom per attached peptide (Figure 5). The signal consists of a broad band with a maximum at 163.2 eV that corresponds to sulfur grafted onto gold, indicating the presence

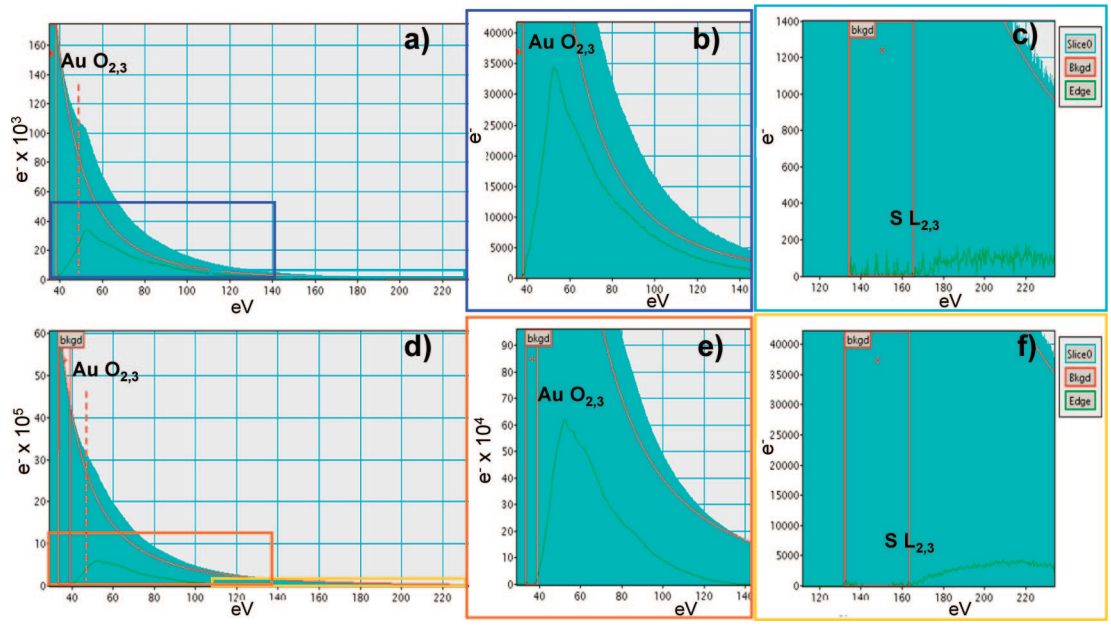

Figure 4. (a) EELS spectrum obtained on the surface of a non-functionalized GNP-20. (b) Detail of the Au $O_{2,3}$ ELNES spectrum bound by the blue rectangle in (a). (c) Detail of the S $L_{2,3}$ edge bound by the cyan rectangle in (a). (d) EELS spectrum obtained on the surface of GNP-20-P1. (e) Detail of the Au $O_{2,3}$ ELNES spectrum bound by the dark orange rectangle in (d). (f) Detail of the S $L_{2,3}$ edge bound by the pale orange rectangle in (d).

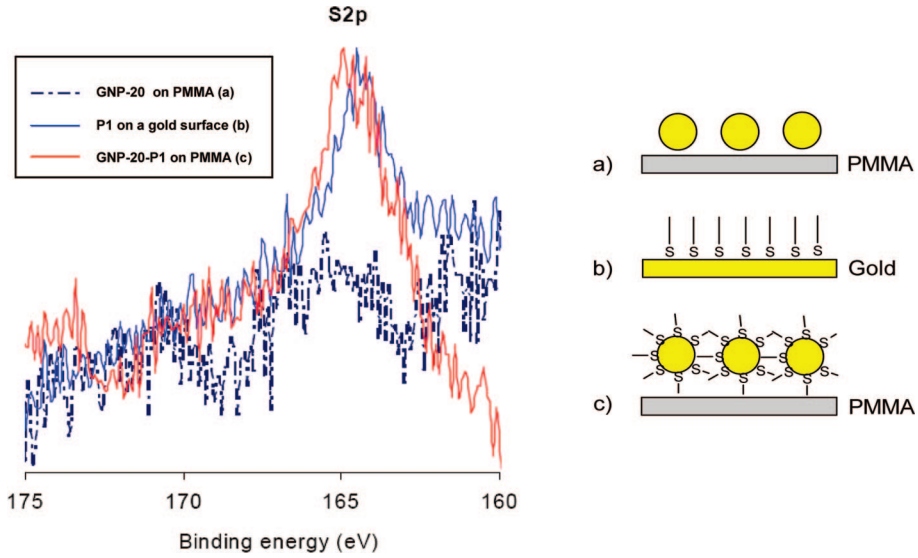

Figure 5. XPS S_{2p} region spectra of (a) GNP-20 on PMMA, (b) **P1**-functionalized gold surfaces, and (c) GNP-20-**P1** on a PMMA surface. The spectra have been normalized.

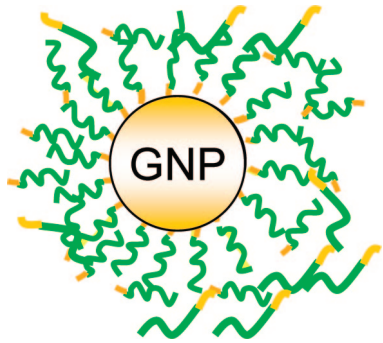

Figure 6. Representation of the functionalization of GNPs with the Kahalalide F analogues and the formation of adlayers. The peptide chain is depicted in green; the thiols belonging to the cysteins are depicted in orange.

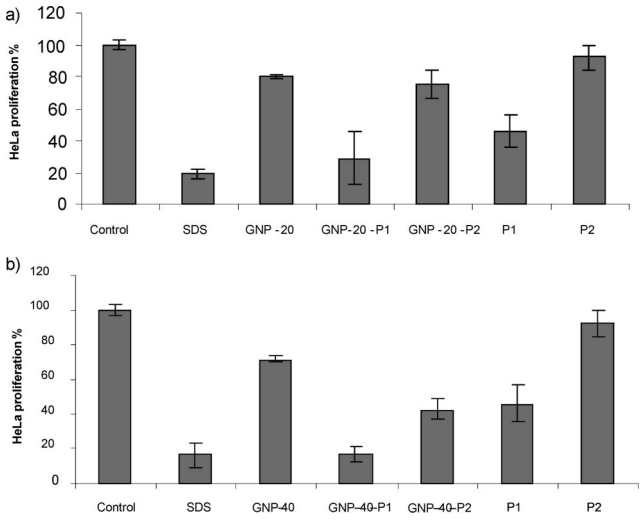

Figure 7. Antiproliferation results of the incubation of **P1-** and **P2-**conjugated 20 nm (a) and 40 nm (b) gold nanoparticles with HeLa cells for 24 h. Cell culture media and SDS were used as negative and positive controls, respectively. The conjugated and nonconjugated peptides were screened against the HeLa cells at a concentration of 1×10^{-5} M. The GNP concentration is the same in all samples.

of Au−S bonds. Although $S_{2p3/2}$ and $S_{2p1/2}$ signals can usually be observed separately, we observed a single broad band, presumably due to shielding of the electron emission by the large peptide. A similar S_{2p} signal was obtained when the peptide was on a non-functionalized gold surface (*57*).

Determination of the Number of Peptide Molecules per GNP. To determine the number of peptide molecules per nanoparticle, nondialyzed aliquots of the conjugated solutions (2.5 mL) were centrifuged at 13 500 rpm for 30 min. The supernatant was lyophilized and then analyzed by HPLC to determine the amount of unconjugated peptide. Approximately 85% of the peptide used in the conjugation was attached to the GNPs. The number of peptides per particle was calculated by dividing the concentration of grafted peptide by the amount of GNPs in solution, which was determined spectrophotometrically considering the molar extinction coefficients detailed in ref *58*. Despite the GNP's size (GPN-20 or GPN-40), the conjugates showed ratios of 60 000 ± 5000 peptide molecules per nanoparticle. However, assuming that the surface of a GNP-20 is 1256 nm^2 or 5024 nm^2 for a GNP-40 and that the surface of a single peptide molecule in an extended conformation is 0.6 nm^2 (data obtained from molecular modeling calculation using the *Insight II* software package), the theoretical number of molecules that would completely cover a GNP-20 surface is only 2090 and 8373 for a GNP-40. This indicated to us that not all peptide molecules were chemisorbed to the nanoparticle surface through the sulfur bond, with the excess of peptide being attached to the nanoparticle by another sort of interaction (Figure 6). One option is the formation of peptide adlayers due to the hydrophobic character of KF, which prompts the assembly of the peptide on the GNP surface in aquous media. Kahalalide F spontaneously self-assembles in aqueous solution, forming spherical supramolecular structures as has been observed by TEM (Supporting Information). This formation of peptide adlayers is a relevant issue to consider when the conjugation of a peptide to a GNP is considered and dramatically influences the final ratio of molecules per nanoparticle, saturating the nanoparticle surface and prompting multilayered capping on the surface. In such a way, the nanoparticles are acting as a concentrator for the delivery of drugs, thereby increasing bioactivity. The influence of the conjugation of **P1** and **P2** on cytotoxic activity was examined as follows.

Cytotoxicity Studies. The degree of cytotoxicity of single peptides (**P1** and **P2**), single GNP solutions (GNP-20 and GNP-40), and their respective conjugates was determined by the WST-1 assay in HeLa tumor cells following 24 h of incubation.

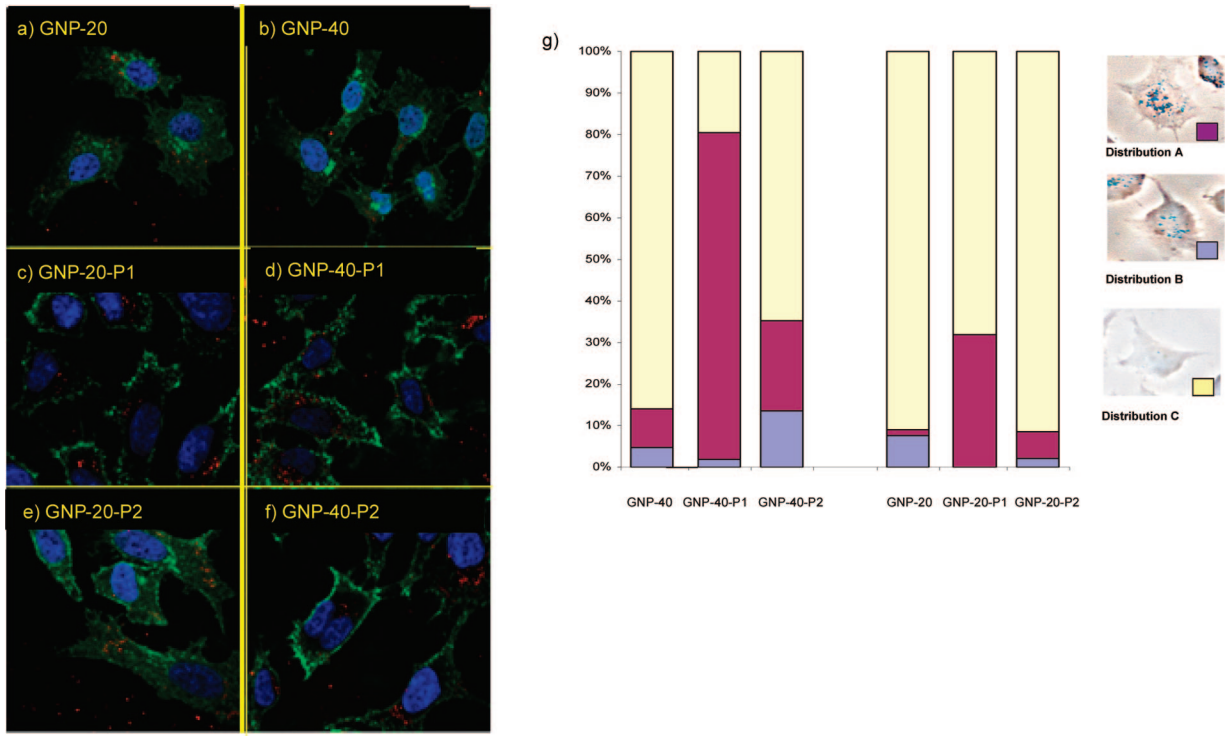

Figure 8. Localization of GNPs and their conjugates in HeLa cells incubated for 24 h (a−f); the red dots represent reflections of groups of nanoparticles. Membranes (green) were stained with a fluorescence marker (WGA), and nuclei (blue) by a DNA marker (Hoechst). Left column: GNP-20. Right column: GNP-40. (g) Percentage of accumulation of GNPs in HeLa cells. The proportion of cells that contain 10 or more reflecting spots (nanoparticules) is represented in burgundy (distribution A). The proportion of cells that contain more than 3 and less than 10 reflecting spots is represented in blue (distribution B). The proportion of cells that contain less than 3 reflecting spots is depicted in yellow (distribution C). The total number of cells taken into account was 100 for each nanoparticle sample.

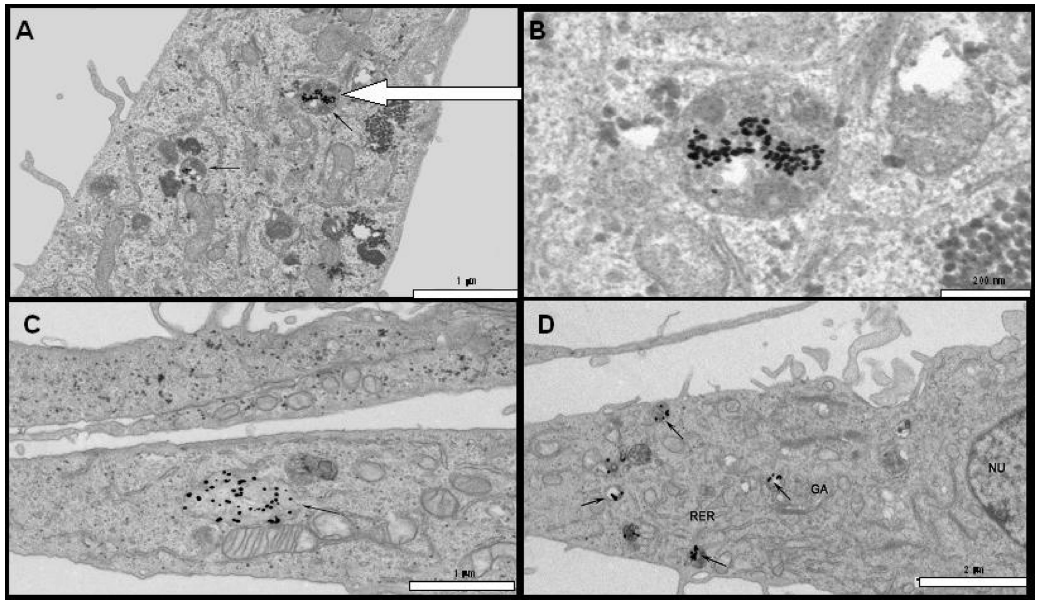

Figure 9. TEM images of HeLa cells incubated with (A) GNP-20-P1. The arrows indicate the presence of the GNPs inside lysosome-like structures. (B) Higher magnification of the accumulated GNP-20-**P1** inside lysosome-like structures. (C) GNP-40-**P1** and (D) bare GNP-20. NU (nucleus), RER (rough endoplasmic reticulum), GA (Golgi apparatus).

Cell culture medium and SDS were considered as negative and positive controls (0% and 80% of inhibition, respectively). The results showed that GNPs displayed residual cytotoxicity against HeLa cells, determined in approximately 22% inhibition for GNP-20 and GNP-40 (Figure 7 and Supporting Information). Regarding the cytotoxicity of single peptides, **P2** was found to be less cytotoxic than **P1** (10% vs 50% inhibition, respectively). The cytotoxicity of conjugates **P1** and **P2** with GNP-20 did not change with respect to the free peptides (Figure 7 and Supporting Information). In contrast, for **P1** and **P2** conjugated with GNP-40 the cytotoxicity is higher with respect to the free peptides (Figure 7). This enhancement could be the result of better cell uptake of the former conjugate, which would be consistent with the findings of Chithrani et al. (*47*). The authors reported that, among nanoparticles of different sizes, those of 50 nm demonstrated the highest level of uptake by HeLa cells. In agreement with these results, Osaki et al. (*59*) qualitatively showed that 50 nm nanoparticles entered the cells via receptor-mediated

endocytosis more efficiently than smaller ones. We attributed the enhanced toxicity of GNP-40-P1 and GNP-40-P2 with respect to **P1** and **P2** to a synergic effect between the peptide and the GNP-40 that favored the penetration and targeting to the lysosome (the putative target of Kahalalide F) (*38*). Confocal and TEM observations to evaluate the accumulation and localization of the conjugates in the cells were carried out.

Cellular Localization of Conjugates. *Accumulation of the Peptide−GNP Conjugates by Confocal Laser Scanning Microscopy (CLSM).* To study the influence of the peptide conjugation on the penetration and distribution of GNPs in cells, both conjugated and unconjugated nanoparticles were observed under confocal microscopy for detection of their reflections. It is important to mention that, in this technique, single GNPs could not be observed; however, if the nanoparticles had been localized together in a cell region, then their detection would have been possible. The cells were fixed with paraformaldehyde and the membranes and nuclei stained. Figure 8 shows how GNPs and peptide−GNP accumulate in cells. Bare GNPs accumulate in cells in low proportion with respect to the conjugates. As expected, the accumulation of GNP-40 is higher than GNP-20, which is in accordance with the results Chitriani et al. (*47*), who hypothesized that GNP uptake is mediated by nonspecific adsorption of serum proteins onto the gold surface; these proteins induce the nanoparticles to enter into cells via the mechanism of receptor-mediated endocytosis. On the other hand, functionalized nanoparticles with peptides presented a higher degree of accumulation in HeLa cells with respect to bare GNPs, with the GNP-40-P1 conjugate showing the highest accumulation. The functionalization of GNPs with **P1** and **P2** introduces a positive charge into the nanoparticle. This charge is achieved by Orn (see Figure 1), which is charged positively at pH = 7.4. This positive charge favors interaction with the membrane (charged negatively) and consequently enhances penetration into the cell. There are several examples in the literature describing the addition of Lys or Arg residues for transfecting molecules into cells (*60, 61*). The lower accumulation of GNPs that are capped with citrate ions in comparison to functionalized nanoparticles could be explained by the fact that the charge of the GNPs is negative (due to the citrate stabilizing ligand). Anionic molecules and structures bind less efficiently to cell surfaces than neutral or cationic molecules, since electrostatic repulsion between the negatively charged surface membrane and cellular environment will repel nanoparticles. Thus, to gain entry, these GNPs must be capped with serum proteins.

Localization of the Conjugates by Transmission Electron Microscopy (TEM). Localization of the peptide−GNP conjugates in the cells was investigated with by TEM. HeLa cells were incubated for 24 h with either conjugated or unconjugated GNPs. TEM images (Figure 9) showed that the penetration of GNP was lower than that of peptide−GNP. Both GNPs and peptide−GNPs were localized in lysosome-like structures. This behavior was not surprising due to lysosomal compartmentalization and was certainly the expected result in most cell uptake processes.

CONCLUSIONS

In summary, conjugating Kahalalide F analogues to GNPs improves the ability of the peptide to target tumoral cell lysosomes (the putative target for Kahalalide F) by using GNPs with high capacity to enter into the cell, thus allowing higher concentrations of peptide molecules which in turn enhances cytotoxicity, as observed for peptides conjugated to GNP-40. The conjugation of bioactive peptides such as Kahalalide F to GNP could be used to direct the drug to the desired pharmacological target, thereby widening the therapeutic index of current cancer therapies. In addition, the peptides conjugated to GNP-40 could find application in treatments based on the destruction of tumoral cells by applying NIR radiation to cells that contain accumulated nanoparticles.

ACKNOWLEDGMENT

This study was partially supported by Chile, FONDAP 11980002 (17070002), FONDECYT 1061142, FONDECYT 7060219; Spain, CICYT (CTQ2006-03794/BQU), ISCIII (CIBER, nanomedicine), MEyC (CENIT, nanopharma), PharmaMar, the Generalitat de Catalunya (2005SGR 00662), the Institute for Research in Biomedicine, and the Barcelona Science Park. M.K. and F.A. give special thanks to AECI for providing a Chile−Spain collaboration grant.

Supporting Information Available: Experimental details. This material is available free of charge via the Internet at http://pubs.acs.org.

LITERATURE CITED

(1) Alivisatos, P. (2004) The use of nanocrystals in biological detection. *Nat. Biotechnol. 22*, 47–52.
(2) Kim, J., Park, S., Lee, J. E., Jin, S. M., Lee, J. H., Lee, I. S., Yang, I., Kim, J. S., Kim, S. K., Cho, M. H., and Hyeon, T. (2006) Designed fabrication of multifunctional magnetic gold nanoshells and their application to magnetic resonance imaging and photothermal therapy. *Angew. Chem., Int. Ed. 45*, 7754–7758.
(3) Katz, E., and Willner, I. (2004) Integrated nanoparticle-biomolecule hybrid systems: Synthesis, properties, and applications. *Angew. Chem., Int. Ed. 43*, 6042–6108.
(4) Krpetic, Z., Porta, F., and Scari, G. (2006) Selective entrance of gold nanoparticles into cancer cells. *Gold Bull. 39*, 66–68.
(5) Panyam, J., Zhou, W. Z., Prabha, S., Sahoo, S. K., and Labhasetwar, V. (2002) Rapid endo-lysosomal escape of poly(D,L-lactide-co-glycolide) nanoparticles: implications for drug and gene delivery. *Faseb J. 16*.
(6) Kogan, M. J., Bastus, N. G., Amigo, R., Grillo-Bosch, D., Araya, E., Turiel, A., Labarta, A., Giralt, E., and Puntes, V. F. (2006) Nanoparticle-mediated local and remote manipulation of protein aggregation. *Nano Lett. 6*, 110–115.
(7) Veiseh, O., Sun, C., Gunn, J., Kohler, N., Gabikian, P., Lee, D., Bhattarai, N., Ellenbogen, R., Sze, R., Hallahan, A., Olson, J., and Zhang, M. Q. (2005) Optical and MRI multifunctional nanoprobe for targeting gliomas. *Nano Lett. 5*, 1003–1008.
(8) El-Sayed, I. H., Huang, X. H., and El-Sayed, M. A. (2005) Surface plasmon resonance scattering and absorption of anti-EGFR antibody conjugated gold nanoparticles in cancer diagnostics: Applications in oral cancer. *Nano Lett. 5*, 829–834.
(9) Jiang, W., Papa, E., Fischer, H., Mardyani, S., and Chan, W. C. W. (2004) Semiconductor quantum dots as contrast agents for whole animal imaging. *Trends Biotechnol. 22*, 607–609.
(10) Berciaud, S., Cognet, L., Blab, G. A., and Lounis, B. (2004) Photothermal heterodyne imaging of individual nonfluorescent nanoclusters and nanocrystals. *Phys. Rev. Lett. 93*, 257402/1–257402/4.
(11) Boyer, D., Tamarat, P., Maali, A., Lounis, B., and Orrit, M. (2002) Photothermal imaging of nanometer-sized metal particles among scatterers. *Science 297*, 1160–1163.
(12) Sonnichsen, C., Franzl, T., Wilk, T., von Plessen, G., Feldmann, J., Wilson, O., and Mulvaney, P. (2002) Drastic reduction of plasmon damping in gold nanorods. *Phys. Rev. Lett. 88*, 077402/1–077402/4.
(13) Yguerabide, J., and Yguerabide, E. E. (2001) Resonance light scattering particles as ultrasensitive labels for detection of analytes in a wide range of applications. *J. Cell. Biochem.* 71–81.
(14) Englebienne, P., Van Hoonacker, A., and Verhas, M. (2001) High-throughput screening using the surface plasmon resonance effect of colloidal gold nanoparticles. *Analyst 126*, 1645–1651.

(15) Karhanek, M., Kemp, J. T., Pourmand, N., Davis, R. W., and Webb, C. D. (2005) Single DNA molecule detection using nanopipettes and nanoparticles. *Nano Lett. 5*, 403–407.
(16) Medintz, I. L., Clapp, A. R., Melinger, J. S., Deschamps, J. R., and Mattoussi, H. (2005) A reagentless biosensing assembly based on quantum dot-donor Forster resonance energy transfer. *Adv. Mater. 17*, 2450–2455.
(17) Taton, T. A., Lu, G., and Mirkin, C. A. (2001) Two-color labeling of oligonucleotide arrays via size-selective scattering of nanoparticle probes. *J. Am. Chem. Soc. 123*, 5164–5165.
(18) Haguet, V., Martin, D., Marcon, L., Heim, T., Stievenard, D., Olivier, C., El-Mahdi, O., and Melnyk, O. (2004) Combined nanogap nanoparticles nanosensor for electrical detection of biomolecular interactions between polypeptides. *Appl. Phys. Lett. 84*, 1213–1215.
(19) Marcon, L., Stievenard, D., and Melnyk, O. (2008) Characterization of nanogap chemical reactivity using peptide-capped gold nanoparticles and electrical detection. *Bioconjugate Chem. 19*, 802–805.
(20) Moller, R., Csaki, A., Kohler, J. M., and Fritzsche, W. (2001) Electrical classification of the concentration of bioconjugated metal colloids after surface adsorption and silver enhancement. *Langmuir 17*, 5426–5430.
(21) Park, S. J., Lazarides, A. A., Mirkin, C. A., Brazis, P. W., Kannewurf, C. R., and Letsinger, R. L. (2000) The electrical properties of gold nanoparticle assemblies linked by DNA. *Angew. Chem., Int. Ed. 39*, 3845.
(22) Park, S. J., Taton, T. A., and Mirkin, C. A. (2002) Array-based electrical detection of DNA with nanoparticle probes. *Science 295*, 1503–1506.
(23) Velev, O. D., and Kaler, E. W. (1999) In situ assembly of colloidal particles into miniaturized biosensors. *Langmuir 15*, 3693–3698.
(24) Kohler, N., Sun, C., Wang, J., and Zhang, M. Q. (2005) Methotrexate-modified superparamagnetic nanoparticles and their intracellular uptake into human cancer cells. *Langmuir 21*, 8858–8864.
(25) Panyam, J., and Labhasetwar, V. (2003) Biodegradable nanoparticles for drug and gene delivery to cells and tissue. *Adv. Drug Delivery Rev. 55*, 329–347.
(26) Yang, P. H., Sun, X. S., Chiu, J. F., Sun, H. Z., and He, Q. Y. (2005) Transferrin-mediated gold nanoparticle cellular uptake. *Bioconjugate Chem. 16*, 494–496.
(27) Chen, J. Y., Wiley, B., Li, Z. Y., Campbell, D., Saeki, F., Cang, H., Au, L., Lee, J., Li, X. D., and Xia, Y. N. (2005) Gold nanocages: Engineering their structure for biomedical applications. *Adv. Mater. 17*, 2255–2261.
(28) Hirsch, L. R., Stafford, R. J., Bankson, J. A., Sershen, S. R., Rivera, B., Price, R. E., Hazle, J. D., Halas, N. J., and West, J. L. (2003) Nanoshell-mediated near-infrared thermal therapy of tumors under magnetic resonance guidance. *Proc. Natl. Acad. Sci. U.S.A. 100*, 13549–13554.
(29) Loo, C., Lin, A., Hirsch, L., Lee, M. H., Barton, J., Halas, N., West, J., and Drezek, R. (2004) Nanoshell-enabled photonics-based imaging and therapy of cancer. *Technol. Cancer Res. Treat. 3*, 33–40.
(30) Daniel, M. C., and Astruc, D. (2004) Gold nanoparticles: Assembly, supramolecular chemistry, quantum-size-related properties, and applications toward biology, catalysis, and nanotechnology. *Chem. Rev. 104*, 293–346.
(31) Wang, Z., Levy, R., Fernig, D. G., and Brust, M. (2005) The peptide route to multifunctional gold nanoparticles. *Bioconjugate Chem. 16*, 497–500.
(32) Levy, R., Thanh, N. T. K., Doty, R. C., Hussain, I., Nichols, R. J., Schiffrin, D. J., Brust, M., and Fernig, D. G. (2004) Rational and combinatorial design of peptide capping Ligands for gold nanoparticles. *J. Am. Chem. Soc. 126*, 10076–10084.
(33) Zharov, V. P., Mercer, K. E., Galitovskaya, E. N., and Smeltzer, M. S. (2006) Photothermal nanotherapeutics and nanodiagnostics for selective killing of bacteria targeted with gold nanoparticles. *Biophys. J. 90*, 619–627.
(34) Zharov, V. P., Galitovskaya, E. N., Johnson, C., and Kelly, T. (2005) Synergistic enhancement of selective nanophotothermolysis with gold nanoclusters: Potential for cancer therapy (vol 37, pg 219, 2005). *Lasers Surg. Med. 37*, 329–329.
(35) Paciotti, G. F., Kingston, D. G. I., and Tamarkin, L. (2006) Colloidal gold nanoparticles: A novel nanoparticle platform for developing multifunctional tumor-targeted drug delivery vectors. *Drug Dev. Res. 67*, 47–54.
(36) Xu, Z. P., Zeng, Q. H., Lu, G. Q., and Yu, A. B. (2006) Inorganic nanoparticles as carriers for efficient cellular delivery. *Chem. Eng. Sci. 61*, 1027–1040.
(37) Janmaat, M. L., Rodriguez, J. A., Jimeno, J., Kruyt, F. A. E., and Giaccone, G. (2005) Kahalalide F induces necrosis-like cell death that involves depletion of ErbB3 and inhibition of Akt signaling. *Mol. Pharmacol. 68*, 502–510.
(38) GarciaRocha, M., Bonay, P., and Avila, J. (1996) The antitumoral compound Kahalalide F acts on cell lysosomes. *Cancer Lett. 99*, 43–50.
(39) Sewell, J. M., Mayer, I., Langdon, S. P., Smyth, J. F., Jodrell, D. I., and Guichard, S. M. (2005) The mechanism of action of Kahalalide F: Variable cell permeability in human hepatoma cell lines. *Eur. J. Cancer 41*, 1637–1644.
(40) Rademaker-Lakhai, J. M., Horenblas, S., Meinhardt, W., Stokvis, E., de Reijke, T. M., Jimeno, J. M., Lopez-Lazaro, L., Martin, J. A. L., Beijnen, J. H., and Schellens, J. H. M. (2005) Phase I clinical and pharmacokinetic study of Kahalalide F in patients with advanced androgen refractory prostate cancer. *Clin. Cancer Res. 11*, 1854–1862.
(41) Hamann, M. T., Otto, C. S., Scheuer, P. J., and Dunbar, D. C. (1996) Kahalalides: Bioactive peptide from a marine mollusk *Elysia rufescens* and its algal diet *Bryopsis* sp. *J. Org. Chem. 61*, 6594–6600.
(42) Pardo, B., Paz-Ares, L., Tabernero, J., Ciruelos, E., Garcia, M., Salazar, R., Lopez, A., Blanco, M., Nieto, A., Jimeno, J., Izquierdo, M. A., and Trigo, J. M. (2008) Phase I clinical and pharmacokinetic study of kahalalide F administered weekly as a 1-h infusion to patients with advanced solid tumors. *Clin. Cancer Res. 14*, 1116–1123.
(43) Spengler, J., Jimenez, J. C., Burger, K., Giralt, E., and Albericio, F. (2005) Abbreviated nomenclature for cyclic and branched homo- and hetero-detic peptides. *J. Pept. Res. 65*, 550–555.
(44) Lopez-Macia, A., Jimenez, J. C., Royo, M., Giralt, E., and Albericio, F. (2001) Synthesis and structure determination of kahalalide F. *J. Am. Chem. Soc. 123*, 11398–11401.
(45) Sagara, T., Kato, N., and Kakashima, N. (2002) Electroreflectance study of gold nanoparticles immobilized on an aminoalkanethiol monolayer coated on a polycrystalline gold electrode surface. *J. Phys. Chem. B 106*, 1205–1212.
(46) Jimenez, J. C., Lopez-Macia, A., Gracia, C., Varon, S., Carrascal, M., Caba, J. M., Royo, M., Francesch, A. M., Cuevas, C., Giralt, E., and Albericio, F. (2008) Structure-activity relationship of kahalalide F synthetic analogues. *J. Med. Chem. 51*, 4920–4931.
(47) Chithrani, B. D., Ghazani, A. A., and Chan, W. C. W. (2006) Determining the size and shape dependence of gold nanoparticle uptake into mammalian cells. *Nano Lett. 6*, 662–668.
(48) Bauer, G., Hassmann, J., Walter, H., Haglmuller, J., Mayer, C., and Schalkhammer, T. (2003) Resonant nanocluster technology - from optical coding and high quality security features to biochips. *Nanotechnology 14*, 1289–1311.
(49) Hogemann, D., Ntziachristos, V., Josephson, L., and Weissleder, R. (2002) High throughput magnetic resonance imaging for evaluating targeted nanoparticle probes. *Bioconjugate Chem. 13*, 116–121.
(50) Liu, J. Q., Zhang, Q., Remsen, E. E., and Wooley, K. L. (2001) Nanostructured materials designed for cell binding and transduction. *Biomacromolecules 2*, 362–368.

(51) Marinakos, S. M., Anderson, M. F., Ryan, J. A., Martin, L. D., and Feldheim, D. L. (2001) Encapsulation, permeability, and cellular uptake characteristics of hollow nanometer-sized conductive polymer capsules. *J. Phys. Chem. B 105*, 8872–8876.

(52) West, J. L., and Halas, N. J. (2000) Applications of nanotechnology to biotechnology - Commentary. *Curr. Opin. Biotechnol. 11*, 215–217.

(53) Link, S., and El-Sayed, M. A. (1999) Size and temperature dependence of the plasmon absorption of colloidal gold nanoparticles. *J. Phys. Chem. B 103*, 4212–4217.

(54) Tkachenko, A. G., Xie, H., Liu, Y. L., Coleman, D., Ryan, J., Glomm, W. R., Shipton, M. K., Franzen, S., and Feldheim, D. L. (2004) Cellular trajectories of peptide-modified gold particle complexes: Comparison of nuclear localization signals and peptide transduction domains. *Bioconjugate Chem. 15*, 482–490.

(55) Olmedo, I., Araya, E., Sanz, F., Medina, E., Arbiol, J., Toledo, P., Alvarez-Lueje, A., Giralt, E., and Kogan, M. J. (2008) How changes in the sequence of the peptide CLPFFD-NH2 can modify the conjugation and stability of gold nanoparticles and their affinity for beta-amyloid fibrils. *Bioconjugate Chem. 19*, 1154–1163.

(56) Usually XPS characterizations are performed on silicon oxide surfaces. Silicon surfaces present two signals corresponding to Si2s and Si2p at 165 and 167 eV, respectively. The Si2s and S2 signals overlapped. The use of PMMA instead of a silicon surface is proposed in the present work in order to avoid interference. XPS characterization of the polymer was performed to discard sulphur impurities.

(57) Barr, T. L. (1994) *Modern ESCA: the principles and practice of X-ray photoelectron Spectroscopy*, CRC Press, Boca Raton, FL.

(58) Jain, P. K., Lee, K. S., El-Sayed, I. H., and El-Sayed, M. A. (2006) Calculated absorption and scattering properties of gold nanoparticles of different size, shape, and composition: Applications in biological imaging and biomedicine. *J. Phys. Chem. B 110*, 7238–7248.

(59) Osaki, F., Kanamori, T., Sando, S., Sera, T., and Aoyama, Y. (2004) A quantum dot conjugated sugar ball and its cellular uptake on the size effects of endocytosis in the subviral region. *J. Am. Chem. Soc. 126*, 6520–6521.

(60) Fernandez-Carneado, J., Kogan, M. J., Pujals, S., and Giralt, E. (2004) Amphipathic peptides and drug delivery. *Biopolymers 76*, 196–203.

(61) Lee, K. D., Nir, S., and Papahadjopoulos, D. (1993) quantitative-analysis of liposome-cell interactions invitro-rate constants of binding and endocytosis with suspension and adherent J774-cells and human monocytes. *Biochemistry 32*, 889–899.

BC800362J